IMP3 RNP safe houses prevent miRNA-directed HMGA2 mRNA decay in cancer and development

Jønson, Lars; Christiansen, Jan; Hansen, Thomas van Overeem; Vikeså, Jonas; Yamamoto, Yohei; Nielsen, Finn Cilius

Published in:
Cell Reports

DOI:
10.1016/j.celrep.2014.03.015

Publication date:
2014

Document version
Publisher's PDF, also known as Version of record

Cell Reports
Article

IMP3 RNP Safe Houses Prevent miRNA-Directed *HMGA2* mRNA Decay in Cancer and Development

Lars Jønson,[1] Jan Christiansen,[2] Thomas V.O. Hansen,[1] Jonas Vikeså,[1] Yohei Yamamoto,[3] and Finn C. Nielsen[1,*]
[1]Center for Genomic Medicine, Rigshospitalet, University of Copenhagen, 2100 Copenhagen, Denmark
[2]Center for Computational and Applied Transcriptomics, Department of Biology, University of Copenhagen, 2200 Copenhagen, Denmark
[3]Department of Molecular Pathology and Tumor Pathology, Akita University, 1-1-1 Hondo, Japan
*Correspondence: fcn@rh.dk
http://dx.doi.org/10.1016/j.celrep.2014.03.015

SUMMARY

The IMP3 RNA-binding protein is associated with metastasis and poor outcome in human cancer. Using solid cancer transcriptome data, we found that *IMP3* correlates with *HMGA2* mRNA expression. Cytoplasmic IMP3 granules contain *HMGA2*, and IMP3 dose-dependently increases *HMGA2* mRNA. *HMGA2* is regulated by *let-7*, and *let-7* antagomiRs make *HMGA2* refractory to IMP3. Removal of *let-7* target sites eliminates IMP3-dependent stabilization, and IMP3-containing bodies are depleted of Ago1-4 and miRNAs. The relationship between *Hmga2* mRNA and IMPs also exists in the developing limb bud, where IMP1-deficient embryos show dose-dependent *Hmga2* mRNA downregulation. Finally, IMP3 ribonucleoproteins (RNPs) contain other *let-7* target mRNAs, including *LIN28B*, and a global gene set enrichment analysis demonstrates that miRNA-regulated transcripts in general are upregulated following IMP3 induction. We conclude that IMP3 RNPs may function as cytoplasmic safe houses and prevent miRNA-directed mRNA decay of oncogenes during tumor progression.

INTRODUCTION

In principle, all posttranscriptional steps can have profound effects on the expression of onco- and tumor-suppressor genes and factors that maintain genome integrity. Although more than 500 different RNA-binding proteins participate in mRNA events, only a handful of these proteins have been directly implicated in neoplasia.

Insulin-like growth factor 2 (IGF2) mRNA-binding protein 3 (IMP3, IGF2BP3) belongs to a family of mRNA-binding proteins (IMP1, IMP2, and IMP3) that are involved in RNA localization, translation, and stability (Christiansen et al., 2009). IMP1 and IMP3 form heterodimers and exhibit similar RNA-binding specificities (Nielsen et al., 2004). They are almost exclusively produced during embryogenesis with early maternal and zygotic expression (for review, see Nielsen et al., 2001), followed by a peak at mouse embryonic days 10.5–12.5 (E10.5–E12.5) (Nielsen et al., 1999; Runge et al., 2000). IMPs are mainly cytoplasmic and form large motile ribonucleoprotein (RNP) granules dispersed around the nucleus and in cellular protrusions (Nielsen et al., 2002). These RNP granules, or "locasomes," are a unique RNP entity distinct from neuronal hStaufen and/or fragile X mental retardation protein granules, processing bodies (P bodies), and stress granules (Jønson et al., 2007). Because granules contain CBP80 and factors belonging to the exon-junction complex, and lack eIF4E, eIF4G, and 60S ribosomal subunits, it is conceivable that mRNAs in these bodies have never been translated.

IMP3 is found in a variety of cancers. IMP3-positive tumors are prone to metastatic behavior and poor outcome (Beljan Perak et al., 2012; Chen et al., 2011, 2013; Hoffmann et al., 2008; Jeng et al., 2008; Jiang et al., 2008b; Kim et al., 2012; Köbel et al., 2009; Li et al., 2011; Lochhead et al., 2012; Lu et al., 2011; Mentrikoski et al., 2009; Schaeffer et al., 2010; Sitnikova et al., 2008; Szarvas et al., 2012; Yantiss et al., 2008), and IMP3 is widely used to depict metastatic tumor cells during staging (Kapoor, 2008; Kim and Cha, 2011; Mentrikoski et al., 2009; Mhawech-Fauceglia et al., 2010; Yantiss et al., 2008). In support of a causal role in transformation, transgenic overexpression of mouse IMP3/KOC leads to increased cell proliferation and metaplasia of pancreatic acinar cells (Wagner et al., 2003), and in mammary-cancer-prone mice, overexpression of IMP1 causes metastatic cancer (Tessier et al., 2004). Although there is clear support for a direct role of IMP3 in tumorigenesis, the mechanisms by which IMP3 elicits its effects are incompletely understood.

To unravel the mechanism by which IMP3 promotes tumor growth, we employed global transcriptome data from a large set of solid cancers, and observed that *IMP3* was correlated with oncogenic *HMGA2* mRNA expression. Similarly to IMP3, HMGA2 is an oncofetal protein that is primarily expressed during embryogenesis (Chiappetta et al., 1996; Zhou et al., 1995). HMGA2 is tumorigenic and associated with poor prognosis and low overall survival (reviewed in Fusco and Fedele, 2007). The *HMGA2* 3′ UTR has considerable potential for posttranscriptional regulation by RNA-binding proteins and miRNA-induced silencing complexes (miRISCs) with its seven *let-7* miRNA target sites in *HMGA2* 3′ UTR (Lee and Dutta, 2007; Mayr et al., 2007).

A

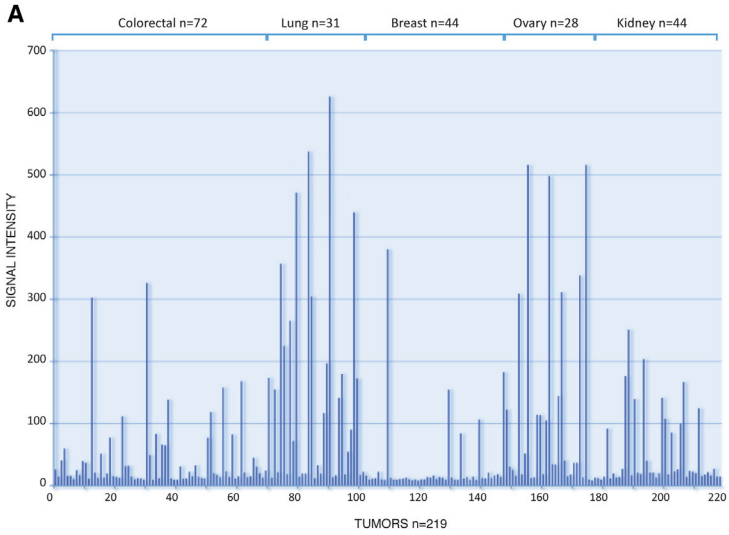

B

Gene Symbol	p-Value	q-Value	Fold change
IGF2BP3	8.4E-58	2.8E-53	9.0
HMGA2	3.7E-15	5.1E-11	3.0
ARNTL2	3.6E-10	4.0E-06	1.7
TOP2A	2.1E-09	1.6E-05	2.9
IGF2BP2	1.4E-08	8.4E-05	2.0
SLC2A1	2.1E-08	1.1E-04	1.8
MTHFD1L	2.6E-08	1.3E-04	1.6
FRMD5	5.9E-08	2.6E-04	1.5
PSAT1	6.1E-08	2.6E-04	2.7

C

Tumor	PC	p-Value	q-Value	t-Value
Breast	0.12	1.0E-3	1.0E-2	3.0
Colorectal	0.23	3.1E-5	3.0E-3	4.2
Kidney	0.36	1.1E-9	3.7E-8	6.3
Lung	0.50	9.7E-13	6.0E-10	7.8
Ovary	0.39	1.2E-8	1.0E-3	5.9
All	0.44	4.9E-54	2.7E-50	16.3

Figure 1. IMP3 in Human Carcinoma

(A) *IMP3* mRNA expression in a series of 270 tumors from lung, kidney, colorectal, breast, and ovary cancers. The data were derived from the IMP3/IGF2BP3 203820_s_at probe set on the Affymetrix 133 Plus 2.0 arrays.

(B) The most enriched transcripts in IMP3-positive tumors as determined by a two-group comparison.

(C) Pearson correlation coefficient between *IMP3* (203820_s_at probe set) and *HMGA2* (208025_s_at probeset) in the different types of cancer, as well as the p value, q value, and t value of the analysis.

We show that IMP3 RNP granules contain large amounts of *HMGA2* transcripts, and that IMP3 locasomes protect and upregulate HMGA2 by opposing the intersection between Ago2/*let-7* and *HMGA2* mRNA. IMP3 RNP granules also contain a number of other *let-7* target mRNAs, including the pluripotency factor *LIN28B* mRNA, that promote tumor growth and embryonal development by inhibiting *let-7* biogenesis. A global gene set enrichment analysis (GSEA) analysis demonstrated that the protective role of IMP3 includes miRNA-regulated transcripts in general. We propose that IMP3 locasomes may function as cytoplasmic safe houses that prevent miRNA-directed mRNA decay of proto-oncogenes during tumor progression and embryogenesis.

RESULTS

IMP3 and HMGA2 mRNA Are Coexpressed in Human Cancers

High levels of RNA-binding IMP3 have been associated with poor outcome and metastasis in cancers of the lung, kidney, colorectal, breast, and ovary (Beljan Perak et al., 2012; Bellezza et al., 2009; Findeis-Hosey et al., 2010; Hoffmann et al., 2008; Jiang et al., 2008a, 2008b; Köbel et al., 2009; Lochhead et al., 2012; Walter et al., 2009; Yuan et al., 2009). To identify putative oncogenic mechanisms connected to IMP3, we examined IMP3 mRNA expression in a series of 270 tumors from the above cancers and searched for transcripts that were correlated with the presence of IMP3.

IMP3 was expressed at high levels in ~45% of the tumors. Compared with background in the negative tumors, IMP3 levels were on average ~6.5-fold higher among positive tumors. Some positive tumors exhibited an up to 40-fold increase in IMP3 (Figure 1A). To identify transcripts that were associated with IMP3 expression, we first employed a two-way comparison of IMP3-positive tumors (>6 IMP3 log2 values) and IMP3-negative tumors (<4.5 IMP3 log2 values) to depict enriched transcripts (Figure 1B). We found that 163 transcripts were enriched in IMP3 tumors after setting a p value cutoff at 1E-10 and a q value of 1E-10. The most enriched transcript encoded *HMGA2* ($p = 1.9 \times 10^{-13}$), followed by *ARNTL2*, *TOP2A*, *IGF2BP2* (*IMP2*), *SLC2A1*, and *MTHFD1L*. The enrichment of IMP2 is in agreement with the fact that HMGA2 promotes transcription of the *IMP2* gene (Brants et al., 2004; Li et al., 2012). A GSEA in the molecular signatures database MSigDB (http://www.broadinstitute.org) showed that IMP3-associated mRNAs overlapped with the Gene Ontology (GO) terms Cell_Cycle_Process ($p = 6 \times 10^{-13}$), Mitotic_Cell_Cycle ($p = 8 \times 10^{-12}$), Spindle ($p = 1 \times 10^{-10}$), and Cell_Cycle_Phase ($p = 6 \times 10^{-10}$), indicating that IMP3-positive tumors, in agreement with previous reports, were characterized by fast proliferation (Hartmann et al., 2012). We subsequently examined a larger collection of 899 cancers from the above groups and showed that the Pearson correlation coefficient between *IMP3* and *HMGA2* among all groups was 0.44 with a false discovery rate (FDR) q value of 2.7×10^{-50}, ranging from 0.12 in breast cancers to 0.5 in lung cancers (Figure 1C). A closer analysis of the breast cancer group showed that the lower correlation in these tumors could be explained by the selective expression of *IMP3* in triple-negative breast cancers, whereas *HMGA2* is also found in other histological classes of breast tumors.

To substantiate the causal relation between IMP3 and HMGA2, we generated a line of HT1080 cells expressing 3xFLAG-tagged IMP3 under control of a tetracycline-inducible promoter, and immunoprecipitated IMP3 RNP after tetracycline

Table 1. List of the 20 Most Upregulated Transcripts after Induction of 3x-FLAG-IMP3

mRNA	Reads	Median Coverage	RPKM	FC +tet versus −tet	FC IP(+tet) versus CL(+tet)	No. of Transcripts	*Let-7* SVR Scores	*let-7* Targetscan
*IMP3**	2,729	34	20.9	16.1	−1.1	–	(−1.1418)	√ (8-mer)
HMGA2	14,139	164	81.6	2.4	8.9	1,720.0	(−0.3281, −0.9940, −0.2490, −0.8742, −0.1048)	√ (8-mer)
IL1B	793	42	18.0	2.1	2.0	75.2	none	
ANKRD46	377	6	3.1	2.1	−1.2	–	(−0.2436)	√ (7-mer-m8)
BACH1	845	26	11.1	2.0	4.0	88.3	(−0.5106, −1.0348)	√ (8-mer)
THBS1	11,330	151	68.4	1.9	−1.2	–	(−0.1594)	√ (7-mer)
S1PR1	597	16	7.0	1.8	2.7	34.9	none	
ZCCHC3	660	17	8.4	1.8	−1.7	–	(−0.9080)	√ (7-mer-m8)
ITGB8	867	7	3.2	1.8	2.2	12.5	(−0.1705)	√ (7-mer-m8)
ARL5B	480	9	4.6	1.8	4.1	33.5	none	
ANKRD1	1,716	69	29.2	1.8	−3.0	–	none	
PLAG1	447	4	2.0	1.8	4.7	16.2	none	
SEMA3A	432	4	2.3	1.7	3.6	14.3	none	
CPA4	2,491	62	29.0	1.7	2.0	95.7	(−0.9174)	√ (8-mer)
TGM2	10,364	193	87.4	1.7	1.4	204.5	none	
TNFRSF11B	332	11	4.5	1.7	1.4	10.6	none	
LIN28B	334	4	1.9	1.7	2.5	8.1	(−0.3931, −0.3511, −0.2389, −0.1497)	√ (8-mer)
IRS2	865	13	7.1	1.6	−1.3	–	(−0.3305)	√ (8-mer)
IL1RAP	650	7	3.5	1.6	1.6	9.0	none	
C9orf6	793	33	14.3	1.6	9.0	208.2	none	

Cultured cells were stimulated with vehicle or tetracycline for 24 hr before total RNA or IMP3 locasomes were isolated. Total RNA and transcripts associated with the IMP3 RNP were subjected to RNA sequencing. The results represent three independent experiments. The table includes the fold change after tetracycline-induction (FC +tet versus –tet) and the fraction of immunoprecipitated reads compared with the number in the initial cell-lysate (FC IP(+tet) versus CL(+tet). Reads, coverage, and number of transcripts are also indicated. The putative *let-7* target sites were identified by submitting the gene symbols to the miRanda or Targetscan databases. The SVR scores of the individual elements are indicated.

induction. Coimmunoprecipitated mRNAs were identified by deep sequencing, and total RNA was also sequenced to determine the relative enrichment of transcripts in IMP3 RNP. A total of 850 transcripts were enriched >3-fold compared with the steady-state levels in HT1080 cells. *HMGA2* was enriched 8.9-fold, and in absolute numbers *HMGA2* mRNA was the most abundant transcript in *IMP3* RNP (Table 1). Taken together, these results demonstrate that *IMP3* and *HMGA2* mRNAs are strongly correlated in solid cancers. Moreover, *HMGA2* mRNA is physically associated with IMP3 RNP in vivo.

IMP3 Upregulates HMGA2 mRNA and Protein

To further substantiate the causal relation between IMP3 and HMGA2, we employed an additional stable HT1080 cell line expressing FLAG-tagged HMGA2 protein. Whereas overexpression of FLAG-HMGA2 protein had no effect on the IMP3 level (data not shown), induction of 3xFLAG-IMP3 (Figure 2A) was followed by a time-dependent rise in the steady-state level of endogenous 4.5 kb *HMGA2* mRNA by a factor of 2.5 after 12 hr (Figure 2B). Similar results were obtained with 3xFLAG-IMP1, which induced *HMGA2* mRNA ~3-fold after 24 hr (Figure S1). There was no indication of alternative *HMGA2* mRNA splicing or poly(A) site usage. Figure 2C summarizes the quantification of the data from the western and northern blot analyses.

To examine whether the increased steady-state level of *HMGA2* mRNA was followed by an increased amount of HMGA2 protein, we performed a western blot analysis in the absence or presence of tetracycline (Figure 2D). Corresponding to the increase in *HMGA2* mRNA, HMGA2 protein levels increased 2.1-fold. Mixing uninduced and tetracycline-induced cells followed by immunocytochemical staining of either nuclear HMGA2 protein (green color) or cytoplasmic 3xFLAG-IMP3 (red color, Figures 2E and 2F) showed that nuclear HMGA2 staining, quantified by confocal microscopy, also was ~2-fold higher in tetracycline-induced cells.

Finally, we determined the translational status of *HMGA2* mRNA following IMP3 induction by means of polysome isolation (Figures 3A and 3B). The analysis provided no indications of altered translational initiation in the presence of IMP3, since *HMGA2* 4.5 kb mRNA sedimented in polysomal fractions 4–8 regardless of tetracycline addition. 3xFLAG-IMP3 was mainly located in subpolysomal fractions 3–5 (Figure 3C).

IMP3 Precludes the HMGA2 and Ago2/let-7 Intersection

HMGA2 mRNA comprises seven putative *let-7* target sites in the 3′ UTR, and regulation of *HMGA2* mRNA decay provides a paradigm for *let-7*-dependent inactivation via the RISC pathway (Boyerinas et al., 2008; Lee and Dutta, 2007; Mayr et al., 2007;

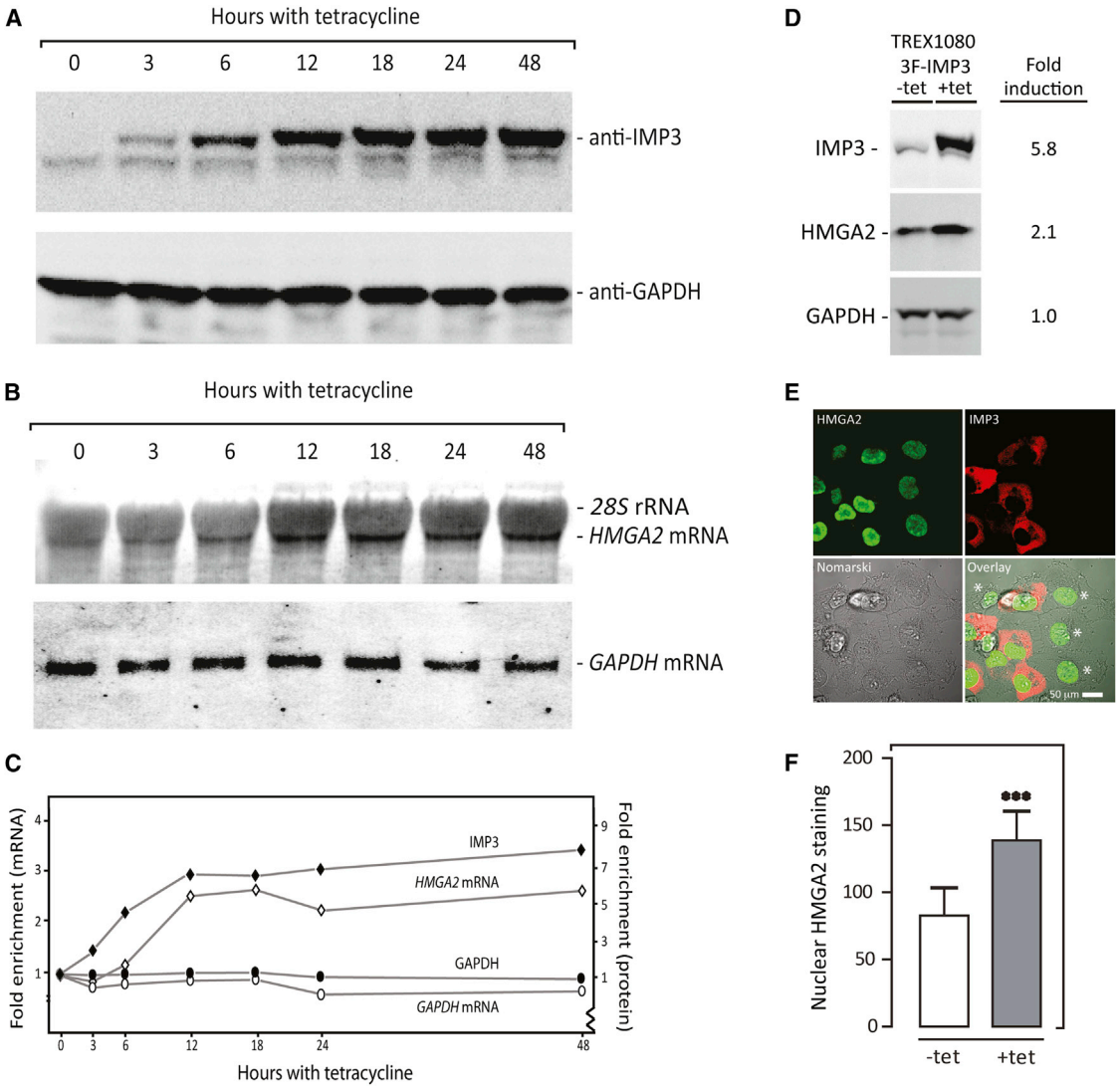

Figure 2. IMP3 Upregulates *HMGA2* mRNA and Protein

(A and B) Time course of steady-state IMP3 protein (A) and *HMGA2* mRNA (B) levels after addition of tetracycline in TREX1080 cells stably expressing 3xFLAG-IMP3. The full-length *HMGA2* transcript of 4.5 kb migrates at the front of the 28S rRNA.

(C) Quantification of the IMP3 protein and the *HMGA2* mRNA content observed after induction of 3xFLAG-IMP3 expression. GAPDH protein and *GAPDH* mRNA content were included as controls in the western blot and northern blot analyses, respectively.

(D) Western blot analysis of IMP3, HMGA2, and GAPDH from TREX1080 3xFLAG-IMP3 cells in the absence (left track) or presence (right track) of tetracycline for 24 hr. The fold change of the protein levels is indicated.

(E) Immunocytochemistry of TREX1080 3xFLAG-IMP3 cells. Tetracycline-stimulated and nonstimulated TREX1080 3xFLAG-IMP3 cells were mixed and plated in a glass bottom dish for 4 hr before they were fixed and stained using FLAG (red) and HMGA2 (green) antibodies. The bottom-right panel depicts the overlay and the bottom-left panel shows the Nomarski rendering. Nonstimulated cells are indicated with asterisks.

(F) Quantification of the nuclear HMGA2 staining in the mixture of cells described in (E). Ten images were processed with the same settings (pinhole, amplification, and exposure time). The cells were depicted as 3xFLAG-IMP3-expressing cells when the red fluorescent signal intensity was >100 arbitrary units. Cells with a red fluorescent signal between 0 and 100 were classified as cells with a leaky tetracycline repressor activity (<5% of the measured cells). The red and green intensities from 80 cells are included in the graph. The error bars represent the SD, and *** represents a p value < 0.0001 using an unpaired Student's t test.

Park et al., 2007). Consequently, we considered whether IMP3 would oppose the actions of *let-7* miRNA on *HMGA2* mRNA.

Segmentation of *HMGA2* mRNA and UV crosslinking with recombinant IMP3 or lysates from uninduced or tetracycline-induced TREX1080 cells initially showed that IMP3 exhibited strong binding to the *HMGA2* 3′ UTR (Figure S2). Endogenous *let-7* isoforms in HT1080 cells were inhibited by a locked nucleic acid (LNA) antagomiR directed toward the *let-7* family in the absence or presence of tetracycline (Figure 4A). A mock transfection or transfection with the unrelated antagomiR anti-miR-449b gave similar results in terms of elevated *HMGA2* mRNA expression following 3xFLAG-IMP3 induction. In

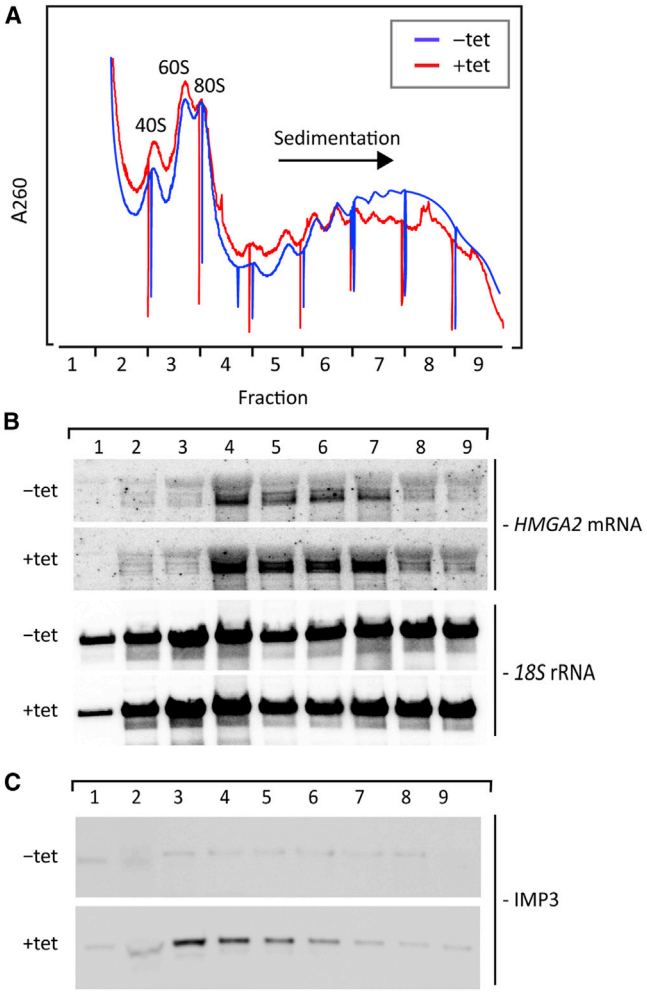

Figure 3. Translation of Endogenous *HMGA2* mRNA following 3xFLAG-IMP3 Induction

(A) A260 profiles of polysomes isolated from exponentially growing TREX1080 cells in the absence or presence of tetracycline.

(B) Northern blot analysis of *HMGA2* mRNA or *18S* rRNA in total RNA isolated from the sucrose gradient fractions. Photon-stimulated luminescence (PSL) minus background (BG) for total *HMGA2* mRNA = 34,598 and 76,346 in the absence or presence of tetracycline, respectively. The corresponding PSL − BG numbers are 1,039,856 and 797,279 for the 18S rRNA signal.

(C) Western blot analysis of IMP3 in the sucrose gradient fractions.

contrast, 3xFLAG-IMP3 was unable to increase the level of endogenous *HMGA2* mRNA beyond the level achieved by removing the *let-7* family, in agreement with a model in which IMP3 increases *HMGA2* expression by opposing *let-7*-mediated decay.

To examine whether the observed effects on the endogenous transcript could be recapitulated in an artificial reporter system with mutated target sites (Figures 4B and 4C), we inserted *let-7* 2&3 and 6&7 target sites into a luciferase reporter vector. Mutating both target sites in the segment with sites 2&3 abolished the effect of 3xFLAG-IMP3, and mutating a single target site in the 6&7 segment was sufficient to eliminate the effect of 3xFLAG-IMP3. In contrast, wild-type versions of segments 2&3 and 6&7 exhibited increased firefly activity upon 3xFLAG-IMP3 induction. We observed a nonadditive effect of 3xFLAG-IMP3 induction both on endogenous *HMGA2* mRNA employing a *let-7* antagomiR and on a luciferase reporter containing mutated *let-7* target sites, implying that IMP3 protects *HMGA2* mRNA from the RISC pathway.

To corroborate the functional significance of IMP3-dependent *let-7* interference, we examined the proliferative capacity of 3xFLAG-IMP3 in the absence or presence of the *let-7* family antagomiR. As shown in Figure 4D, the number of cells that overexpressed IMP3 began to increase 10–12 hr following the addition of tetracycline. This coincided with the increase of the *HMGA2* transcript, which was visible after 6 hr of tetracycline treatment and continued to increase for an additional 10 hr (Figures 2B and 2C). The effect of 3xFLAG-IMP3 expression on the doubling time was similar to that observed after addition of the *let-7* family antagomiR, and the two treatments were not additive. The reduction in doubling time upon 3xFLAG-IMP3 addition is 13%, which will generate a 74-fold difference in tumor volume after 1 month (720 hr). Knockdown of *HMGA2* mRNA was followed by a clear inhibition of cell proliferation and eliminated the effect of IMP3 (Figure 4E).

IMP3 Locasomes Provide a RISC-Free Cytoplasmic Repository for HMGA2 mRNA

Because the luciferase reporter assay of *HMGA2* 3′ UTR segment 2&3 in Figures 4B and 4C showed that downregulation of luciferase expression by *let-7* miRNA could be partially rescued by IMP3, we examined the possibility of a direct competition between *let-7*g miRNA and IMP3 for the *HMGA2* segment 2&3 (3′ UTR positions 1,088–1,306). The electrophoretic mobility-shift analysis shown in Figure 5A indicates that recombinant IMP3 is able to associate with radiolabeled segment 2&3 with a K_d of ~1 nM, and the analysis in Figure 5B reveals that radiolabeled *let-7*g miRNA is able to associate with its target RNA in segment 2&3, regardless of the presence of IMP3. To pinpoint the interactions between the three species at the nucleotide level, we carried out a selective 2′-hydroxyl acylation analyzed by primer extension (SHAPE) analysis of segment 2&3 RNA (McGinnis et al., 2012). Figure 5C shows that in the presence of IMP3 alone, acylations are enhanced in the seed target region, whereas in the presence of *let-7*g miRNA, acylations are blocked due to duplex formation between the *let-7*g seed region and its target, regardless of the presence of IMP3. In contrast, outside the seed target region in segment 2&3, the acylation behavior is dictated by IMP3 rather than *let-7*g miRNA. We infer that IMP3 and *let-7*g miRNA are able to associate simultaneously with *HMGA2* segment 2&3 in vitro, so the opposing effect observed in vivo is unlikely to result from a straightforward competition between *let-7*g miRNA and IMP3 for the *HMGA2* 3′ UTR seed target.

Because upregulation of *HMGA2* mRNA was unlikely to result from a direct sterical hindrance of *let-7* miRNA binding, we examined whether IMP3 RNP represents a RISC-free environment. Immunoprecipitations of cytoplasmic lysates in the presence of 0.5 mM EDTA with Ago2 or FLAG antibodies (Figure 6A) revealed that endogenous full-length *HMGA2* mRNA was virtually undetectable in the anti-Ago2 immunoprecitate. The

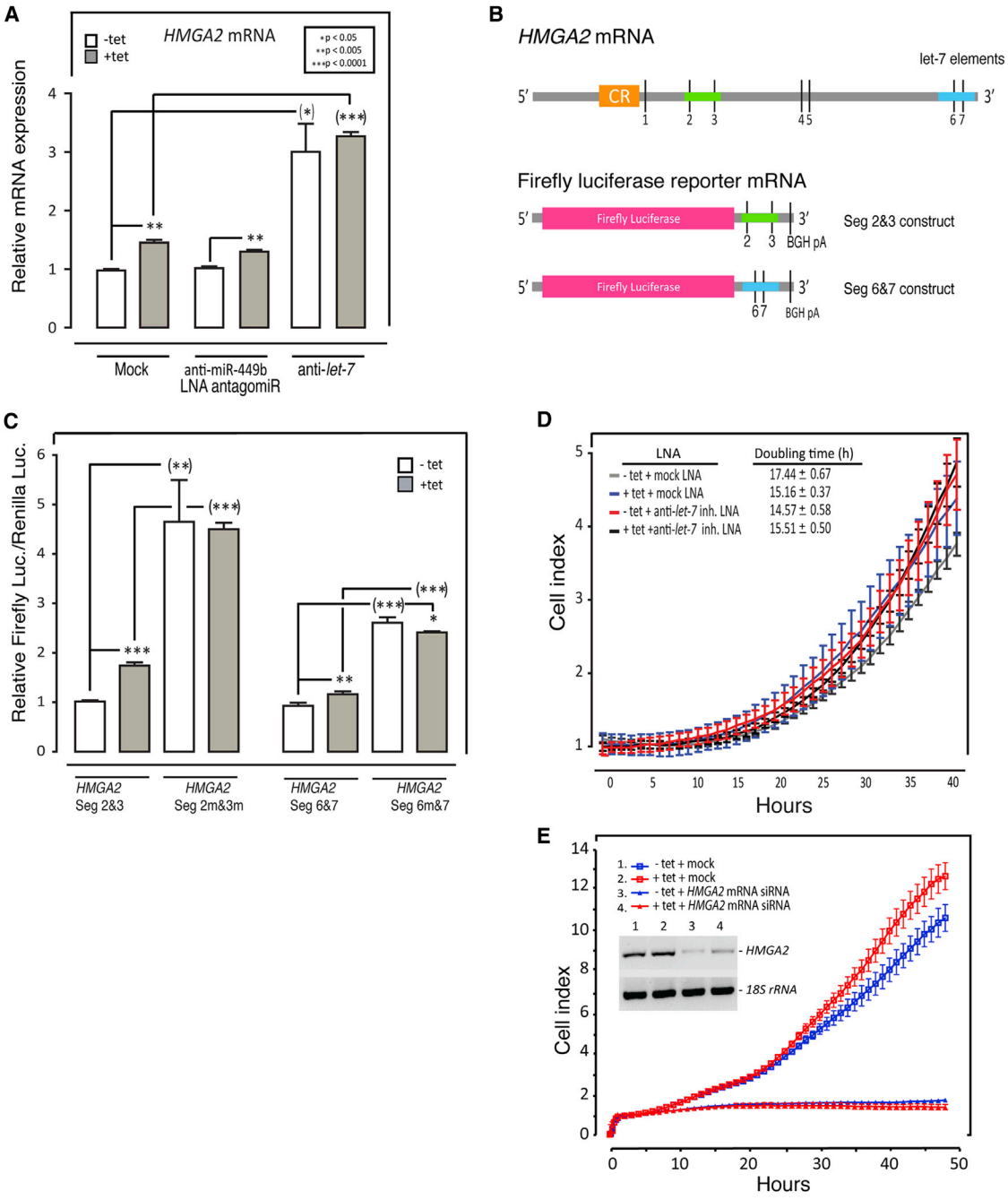

Figure 4. IMP3-Induced Increase of *HMGA2* mRNA Depends on *let-7* miRNA

(A) Endogenous *HMGA2* mRNA levels after 3xFLAG-IMP3 induction in the presence of mock, anti-*miR-449b*, or anti-*let-7* LNA antagomiR. The LNA miCurry inhibitors were transfected 16 hr before the cells were split and cultured in media with or without tetracycline. The data represent three independent experiments and are presented as mean ± SD.

(B) Schematic representation of full-length *HMGA2* mRNA and the firefly luciferase reporter constructs encompassing two *let-7* target sites 2&3 (green) and 6&7 (blue) examined in the absence or presence of 3xFLAG-IMP3. Colored boxes depict reading frames, UTRs are depicted as gray lines, and 2&3 and 6&7 designate RNA segments that exhibit strong IMP3 binding. In addition to the two wild-type segments inserted downstream of firefly luciferase, two other constructs were made in which two nucleotides in the seed target sequence (UACCUC→UGCGUC) were mutated.

(C) Activation of the luciferase reporters outlined in (B) by 3xFLAG-IMP3 in the presence of intact or mutated *let-7* target sequences. The y axis represents the relative firefly luciferase activity divided by the *Renilla* luciferase activity. In the segment 2&3 construct, both *let-7* target sites were mutated (*HMGA2* Seg 2 m&3 m), whereas only the biologically active target site was mutated in the segment 6&7 construct (*HMGA2* Seg 6 m&7). The data originate from three independent experiments and are presented as the mean ± SD.

(legend continued on next page)

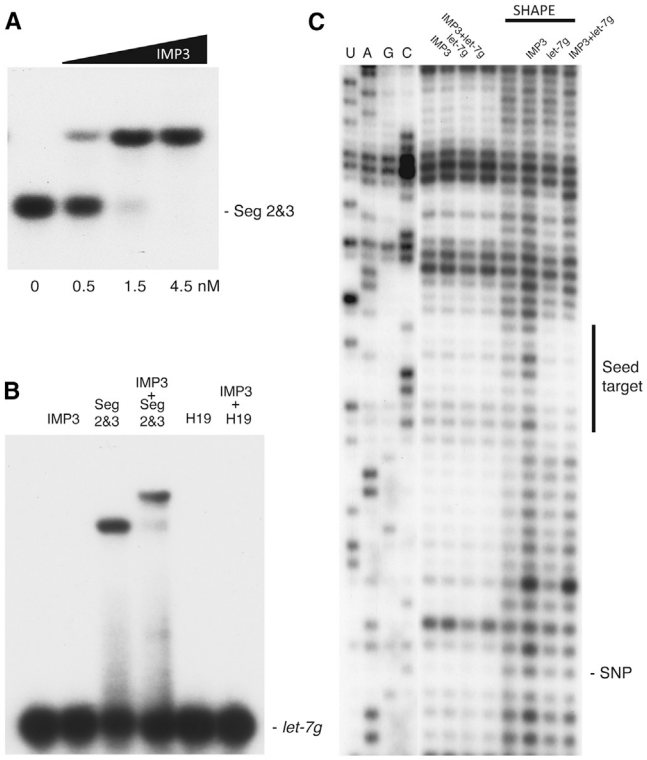

Figure 5. IMP3 and *let-7g* miRNA Associate Simultaneously with an *HMGA2* 3′ UTR Segment Encompassing Target Site 3 In Vitro

(A) Electrophoretic mobility shift assay of ^{32}P-labeled 3′ UTR segment 2&3 (positions 1,088–1,306) with increasing concentrations of recombinant IMP3.

(B) Electrophoretic mobility shift assay of 5′[^{32}P]-*let-7g* miRNA with recombinant IMP3, unlabeled 3′ UTR segment containing target site segment 2&3, or a combination of IMP3 and the 3′ UTR segment. *H19* is a similar-sized unlabeled RNA that exhibits IMP3 attachment.

(C) SHAPE analysis of a 3′ UTR segment containing target site 2&3 on its own, in combination with either IMP3 or *let-7g*, or in the presence of both. U, A, G, and C designate dideoxynucleoside sequencing tracks, and the middle four tracks derive from samples that have not been exposed to the 1M7 reagent. The vertical bar brackets the positions complementary to 2–8 in *let-7* miRNA. The SNP rs1042725 is the C/T polymorphism associated with height in GWA studies.

abundance of *let-7* miRNAs implied an intact RISC particle, at least in terms of the interaction between Ago2 and miRNA. In contrast, the full-length *HMGA2* mRNA was abundantly present in the 3xFLAG-IMP3 immunoprecipitate, even to the extent that it was visually diminished in the nonbound material. Moreover, the absence of Ago2 in the anti-FLAG immunoprecipitate (and vice versa) shows that RISC particles and IMP3 RNPs are distinct entities with little overlap from a biochemical point of view. Finally, as described above, eIF4E was absent from IMP3 RNP. To corroborate the biochemical observations, we performed immunocytochemistry with iMP3, Ago2, and DCP1a antibodies (with the latter staining P bodies). Confocal microscopy showed that there was no overlap between anti-iMP3 and either anti-Ago2 or anti-DCP1a stainings, reinforcing the biochemical observations (Figure 6B). Similar results were obtained following analysis of Ago1, Ago3, and Ago4 with respect to both coimmunoprecipitation and cellular distribution (Figure S3). Moreover, we examined the presence of miRNAs in RNA from total lysates or 3xFLAG-IMP3 and 3xFLAG-RRM1-2 (negative control) immunoprecipitates by global miRNA microarray analysis (Figure S4). This demonstrated that miRNAs were excluded from the IMP3 granules. No statistical difference was observed between IMP3 and RRM1-2 isolates (FDR > 0.2). Taken together, these data imply that IMP3 RNPs provide a cytoplasmic domain that is devoid of components of the RISC pathway.

Let-7 Targets in IMP3 RNP Granules

IMP3 locasomes have been proposed to represent posttranscriptional regulons (Jønson et al., 2011). To generalize our observations concerning IMP3 and miRNA activity, and reveal additional transcripts that could play a role in cancer progression, we compared global RNA sequencing profiles from cells treated with and without tetracycline with the transcripts identified in the particles. Among the 20 most upregulated transcripts, eight of 19 (excluding IMP3) exhibited *let-7* seed target sequences according to the miRanda database, and nine of 19 exhibited them when we employed Targetscan to predict the targets. As shown in Table 1, the *HMGA2* transcript was the most upregulated transcript (2.4-fold) upon IMP3 induction, followed by *ANKRD46*, *BACH1*, *THBS1*, *ZCCHC3*, *ITGB8*, *CPA4*, *IRS2*, and *LIN28B*. *HMGA2* was strongly enriched (9-fold) in the particles together with *let-7* target-containing *BACH1*, *ITGB8*, *CPA4*, and *LIN28B*. A number of the remaining enriched transcripts were targets for other miRNAs, in particular miR-181a/b (data not shown).

RNA-binding *LIN28B* blocks the nuclear conversion of the primary *let-7* transcript to pre-*let-7* (Heo et al., 2008; Viswanathan et al., 2008), and LIN28B promotes malignant growth by opposing *let-7* (Viswanathan et al., 2009). Moreover, LIN28B is expressed at the same developmental stages as IMPs (Yang and Moss, 2003) and controls body size similarly to HMGA2 and IMP1 (Shinoda et al., 2013). Therefore, we considered whether IMP3 locasomes represent a regulon that integrates the expression of *LIN28B* and *HMGA2* by opposing *let-7*. We

(D) Removal of *let-7* opposes the mitogenic actions of IMP3. TREX1080 cells stably expressing 3xFLAG-IMP3 were transfected with an LNA antagomiR against the *let-7* miRNA family and a mock control. Half of the transfected cells were grown in the absence or presence of tetracycline to induce 3xFLAG-IMP3 expression, followed by seeding in E-plates (Roche) and measurement of cell growth in an xCELLigence apparatus. The number of cells was set to one (cell index) at 0 hr to normalize for differences in plating. The data represent three independent measurements and are presented as mean ± SD.

(E) *HMGA2* is essential for cell proliferation. TREX1080 cells stably expressing 3xFLAG-IMP3 were transfected with a small interfering RNA (siRNA) against *HMGA2* and a control siRNA. After transfection, cells were grown in the absence or presence of tetracycline to induce 3xFLAG-IMP3 expression, followed by seeding in E-plates (Roche) and measurement of cell growth in an xCELLigence apparatus. The number of cells was set to one (cell index) at 0 hr to normalize for differences in plating. The data represent three independent measurements and are presented as mean ± SD. Quantitative PCR of the cellular *HMGA2* mRNA and *18S* rRNA content was performed after siRNA transfection and visualized by gel electrophoresis.

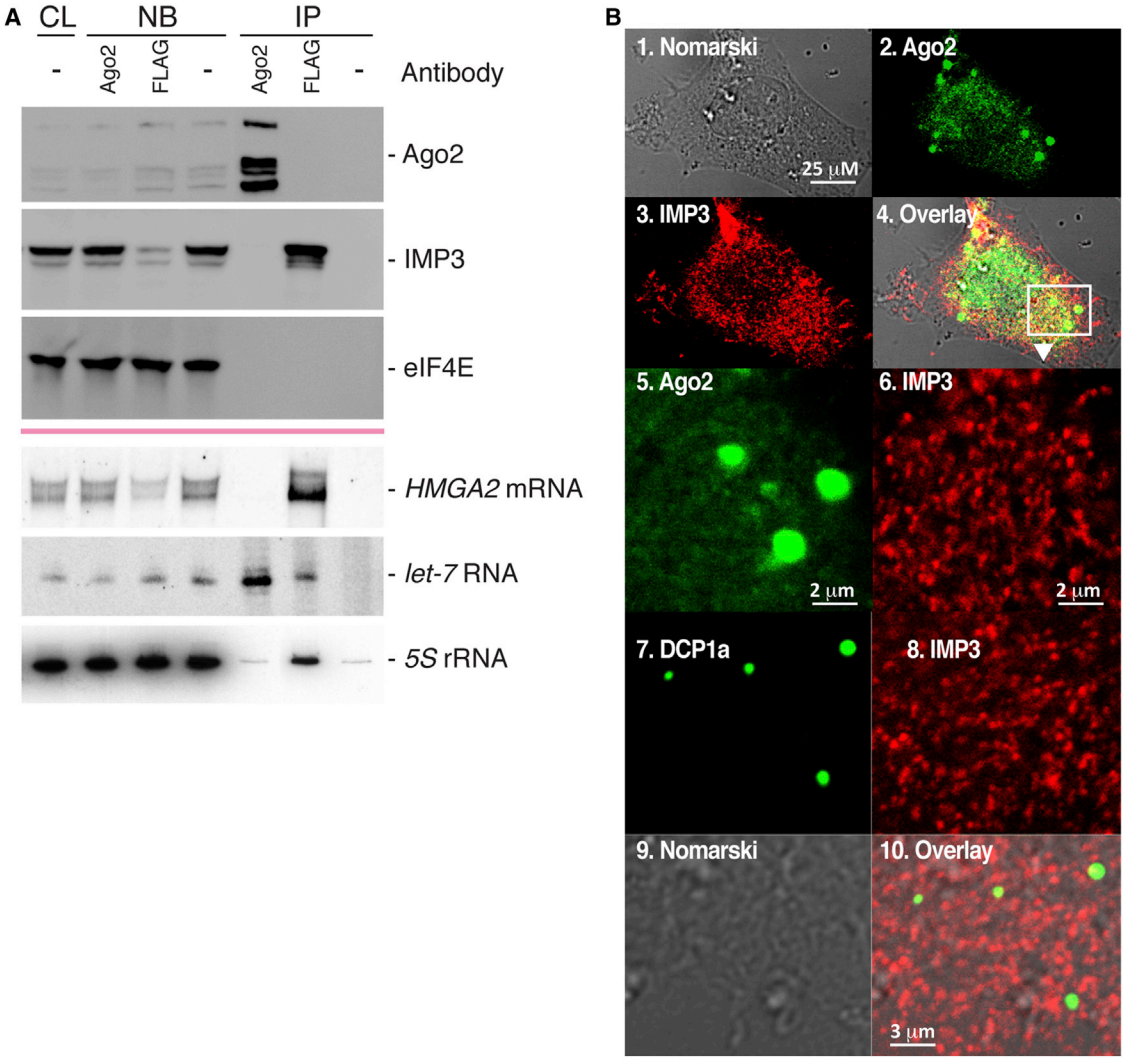

Figure 6. IMP3 Locasomes Are RISC-Free Repositories for *HMGA2* mRNA

(A) TREX1080 cells stably expressing 3xFLAG-IMP3 were lysed and aliquoted for subsequent immunoprecipitations with antibodies against Ago2 or the FLAG-tag. Total cell lysate (CL) and proteins that were not bound to the beads (NB) or immunoprecipitated proteins (IP) were analyzed by western blot analysis (upper three panels) with the indicated antibodies against Ago2, IMP3, or eIF4E. Negative controls (−) depicted in tracks 4 and 7 show the result from protein-G-coated beads without a conjugated antibody. Northern blot analyses using probes against the open reading frame of *HMGA2* mRNA, *let-7* miRNAs, or 5S rRNA are shown in the bottom three panels. The immunoprecipitated material corresponded to 32 times the input.

(B) Immunocytochemical analysis of IMP3 locasomes and P bodies. Cells were cultured in glass-bottom dishes, fixed, and incubated with anti-Ago2 (panels 2, 4, and 5), anti-DCP1a (panels 7 and 10) and anti-FLAG (panels 3, 4, 6, 8, and 10) antibodies, and secondary antibodies before they were examined by confocal microscopy. Nomarski pictures are included to provide an overview of the cells. Blowouts are marked by the square and arrow, and are depicted in panels 5 and 6.

examined the effect of IMP3 and *let-7* antagomiRs on *LIN28B* mRNA expression (Figure S5), and found that similarly to *HMGA2* mRNA, *LIN28B* mRNA was induced ~2-fold after 3xFLAG-IMP3 induction. *Let-7* antagomiRs increased the steady-state level of LIN28B mRNA 3-fold, and it was not possible to impose a further increase of the *LIN28B* transcript following addition of 3xFLAG-IMP3. MiR-449, which was included as a control, had no effect on the *LIN28B* mRNA level. For comparison, we also examined the effects of 3xFLAG-IMP3 and *let-7* antagomiRs on IMP1 expression. *IMP1* mRNA exhibits *let-7* target sites in the 3′ UTR (Boyerinas et al., 2008), but in contrast to *HMGA2* and *LIN28B* mRNAs, the transcript is not associated with IMP3 RNP. In agreement with a protective activity of granule association, *IMP1* mRNA was not increased upon induction of 3xFLAG-IMP3, whereas addition of *let-7* antagomiRs increased the level of *IMP1* transcripts.

To examine whether IMP granules exhibit a more generalized protection of miRNA-targeted mRNAs, we generated a list of miRNA-regulated mRNAs by combining Targetscan predictions with the expression of miRNAs and mRNAs as described

previously (Gallagher et al., 2010). To validate the list of putative miRNA targets, we first performed a GSEA with the 1,000 transcripts that were predicted to be most repressed in HEK293 cells in a previous *Ago2* knockdown analysis from Schmitter et al (2006) (Figure S6A). This showed that the predicted miRNA-regulated transcripts were clearly enriched following *Ago2* knockdown.

To study whether IMP1 or IMP3 imposed a global protection against miRNAs, we performed GSEAs using the top 300 miRNA-regulated mRNAs in the two-group comparisons of tetracycline-induced 3xFLAG-IMP1 HT1080 cells (Figure S6B), 3xFLAG-IMP3 HT1080 cells (Figure S6C), and 3xFLAG-IMP1 HEK293 cells (Figure S6D) versus noninduced cells. In all cases, we observed a significant ($p < 0.001$) enrichment of the miRNA-repressed mRNAs following IMP overexpression. As expected, not every miRNA-targeted transcript became upregulated, conceivably because IMPs bind different mRNAs with varying affinity. We therefore examined whether transcripts that were highly embedded in the granules would be insensitive to *Ago2* knockdown compared with transcripts in which only a small fraction of the total pool was bound to IMP granules. The analysis showed that tightly associated mRNAs were unresponsive to *Ago2* knockdown (NES = −0.92, p = 0.549) (Figure S6F), whereas less-granule-associated mRNAs were enriched following *Ago2* depletion (NES = 1.42, p = 0.002) (Figure S6E), in agreement with a model in which granule-associated mRNAs, in general, are less accessible to the RISC complex. Taken together, these results indicate that IMP1 and IMP3 granules provide a generalized protection against miRNA-mediated mRNA decay.

Interplay among Hmga2 mRNA, let-7 miRNA, and IMP1 during Limb Bud Development

To establish whether the effects observed in HT1080 cells also occurred in the intact organism, we directed our attention toward the developing mouse. Figure 7A is a schematic outline of the reciprocal expression of *Hmga2* mRNA and *let-7* miRNA during mouse development (Park et al., 2007) upon which the narrow temporal expression of the IMP family has been superimposed (Nielsen et al., 1999). Characteristically, IMPs are present at the stage where there is a sharp posttranscriptional downregulation of *Hmga2* mRNA mediated by increasing amounts of *let-7* miRNA. Therefore, it ought to be feasible for IMPs to adjust the expression of *Hmga2*, provided a similar spatial expression pattern is observed.

IMP1 and IMP3 exhibited similar binding to *HMGA2* segment 2&3 and segment 6&7 (Figure 7B), and, as described above, both factors induced *HMGA2* to the same extent (Figure S1). We employed *Imp1* mice because IMP1 is the dominant fetal isoform, whereas IMP3 is predominantly expressed during carcinogenesis. In situ hybridizations with either an *Imp1* probe (Figure 7C, pictures 1 and 2) or an *Hmga2* probe (Figure 7C, pictures 3 and 4) at E12.5 showed overlapping staining with both probes in the limb bud. Therefore, limb buds from wild-type *Imp1*, heterozygous *Imp1*/−, and knockout −/− mice were examined at E13.5 and E14.5 to achieve different concentrations of IMP1 protein. In parallel, quantification of a northern blot analysis of full-length *Hmga2* mRNA revealed that there was a dose-dependent decrease in the *Hmga2* mRNA level upon IMP1 depletion (Figures 7D and 7E). We infer that the interplay between *HMGA2* mRNA and the IMP RNA-binding protein family, as seen in a human cancer cell line, is also present in the developing limb bud in the mouse.

DISCUSSION

To search for molecular targets of IMP3, we employed a large number of genome-wide expression profiles from different solid tumors and searched for mRNAs that were correlated with *IMP3* expression. This approach is appealing because it requires no a priori assumption of possible interactions. Moreover, the data reflect the situation in real solid tumors. We discovered a positive association between *HMGA2* and *IMP3*, which we examined further because *HMGA2* is a well-established oncogene and overlaps temporally and spatially with IMP3 during embryogenesis (Cleynen and Van de Ven, 2008).

IMP3 was physically associated with and upregulated *HMGA2* mRNA and protein, with no apparent effect on translation initiation. Since IMP3 resides in stable cytoplasmic RNP granules, it was conceivable that IMP3 stabilized *HMGA2* mRNA. This let us to examine the effect of IMP3 on *let-7*-dependent downregulation of *HMGA2* mRNA. Although RNA-binding proteins such as IMPs may affect miRNA binding (Elcheva et al., 2009) and miRNA biogenesis, or alter the secondary structure of miRNA target sites (reviewed in van Kouwenhove et al., 2011), we were unable to reveal a straightforward competition between IMP3 and *let-7* for a common *cis* element. Instead, our results point toward an additional possibility that has implications for our understanding of mRNA locasomes/granules. Both the immunoprecipitation and colocalization experiments showed little, if any, overlap between IMP3 and Ago2, which is compatible with distinct cytoplasmic domains for IMP3 and Ago2. In this way, IMP3 locasomes may be regarded as safe houses for mRNAs, where they are protected from degradation on the way to their final destinations and translation. As mentioned above, transcripts have not completed their pioneering round of translation, so it is appealing to regard locasomes as an extension of the nuclear compartment in the cytoplasm.

The physical details of IMP granules, and RNP granules in general, are beginning to emerge. Recent studies of synaptic RNP granules have shown that they exit the nucleus by budding through the inner and outer membranes via a nuclear egress mechanism (Speese et al., 2012). Aggregation and recruitment into condensed hydrogels are likely to occur through polymerization of low-complexity sequences present in RNA-binding proteins (Han et al., 2012; Kato et al., 2012). In agreement with these observations, IMP granules are dynamic and exhibit a diameter in the range of 100–300 nm. Particles may contain several hundred protein molecules roughly the size of IMPs and 10–30 mRNA transcripts (Jønson et al., 2007), and their "nuclear" status is supported by the presence of PABN1/PABP-2 (Speese et al., 2012). It remains to be resolved how Ago2/RISC is excluded from the locasomes, but a combination of sterical hindrance by the dense protein core and a lack of low-complexity sequences that are required for sustained association with the particles (Weber and Brangwynne, 2012) may play a role.

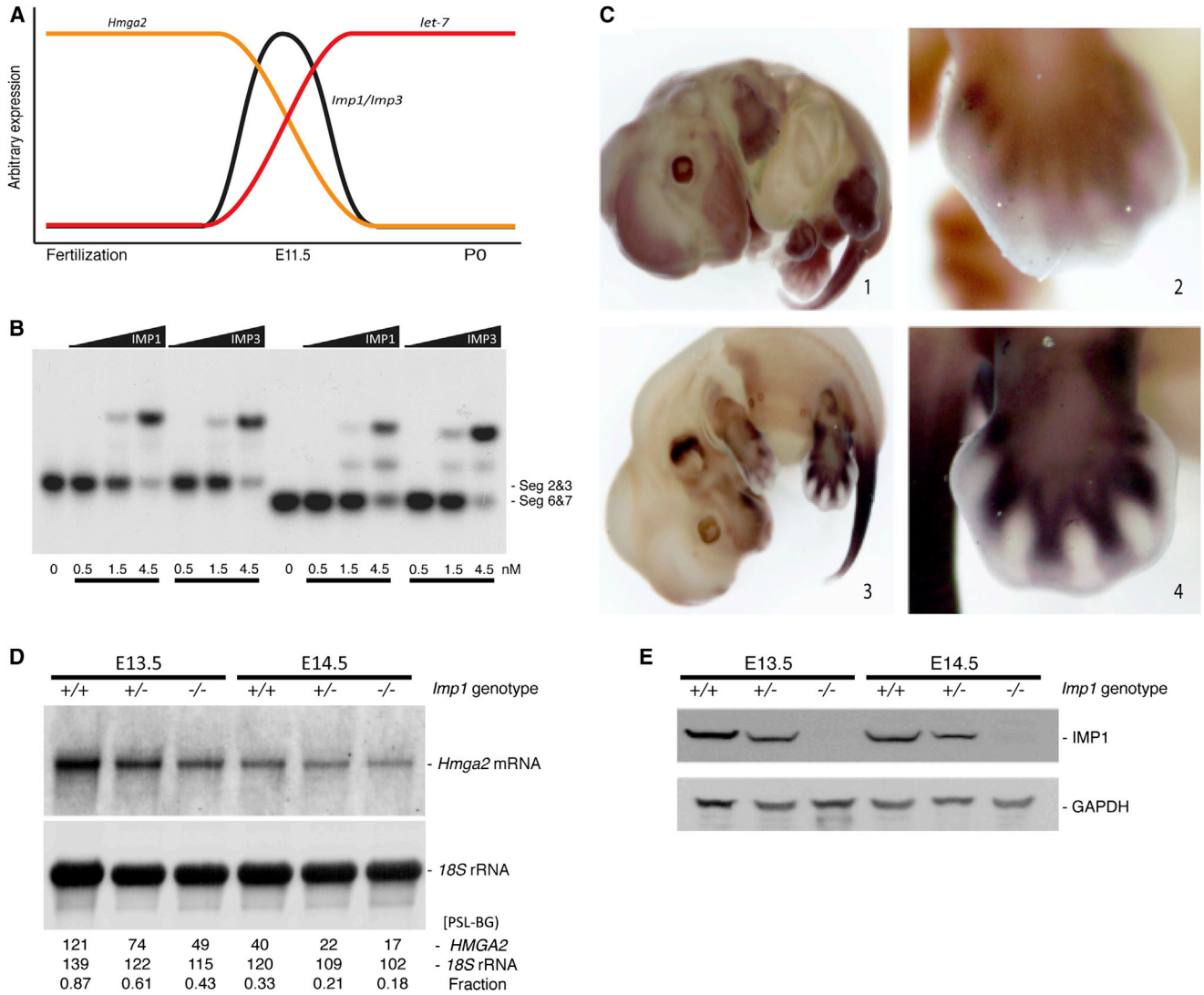

Figure 7. The Mouse *Hmga2* mRNA Level Correlates with IMP1 Protein Expression during Limb Bud Development

(A) Schematic outline of the *Imp1/3*, *Hmga2*, and *let-7* RNA levels during mouse development.

(B) Electrophoretic mobility shift analysis of 3′ UTR segments 2&3 and 6&7 with recombinant IMP1 and IMP3.

(C) Whole-mount in situ hybridizations with DIG-labeled *Imp1* probes (panels 1 and 2) and *Hmga2* probes (panels 3 and 4).

(D) Northern blot analysis of total RNA isolated from limb buds of a wild-type mouse embryo, a heterozygotic *Imp1*/– embryo, and an *Imp1* knockout embryo at E13.5 and E14.5. The PSL is indicated below.

(E) Western blot analysis shows the IMP1 and GAPDH protein levels within the limb buds used for the northern blot analysis.

Several transcripts in the locasomes contained *let-7* target sites (Dogar et al., 2014; Hu et al., 2013; Yun et al., 2011; Zhu et al., 2011) and became upregulated upon IMP3 induction. One of these was *LIN28B* mRNA, which, similarly to IMP3 and HMGA2, has been implicated in various developmental processes and cancer (reviewed by (Thornton and Gregory, 2012). LIN28B blocks the production of mature *let-7* miRNA (Heo et al., 2008; Viswanathan et al., 2008), and this promotes malignant growth (Molenaar et al., 2012; Viswanathan et al., 2009). In humans and mice, IMP3/IMP1, HMGA2, and LIN28B are involved in growth and differentiation, and the deletion of either factor in mice leads to dwarfism (Hansen et al., 2004; Shinoda et al., 2013; Zhou et al., 1995). The physiological significance of the intersection is illustrated by the lowered *Hmga2* mRNA levels in the E13.5 limb buds of our *Imp1* knockout mice, which emphasizes the critical importance of RNA-binding protein concentration in the intact organism. *LIN28B* mRNA is coexpressed with members of the IMP family during midgestation, particularly in epithelia (Yang and Moss, 2003), and *LIN28B* mRNA is also coexpressed with *IMP3* mRNA in a number of cancers (data not shown). Therefore, taken together, our findings indicate that the activity of *HMGA2*, *LIN28B*, and *let-7* is coordinated by heterochronic IMP3 during embryogenesis and carcinogenesis.

Taken together, the IMP3-mediated alleviation of *let-7* activity toward *HMGA2* and *LIN28B* mRNAs may explain why poor outcome is a hallmark of IMP3-positive tumors. Moreover, our data demonstrate how posttranscriptional mechanisms may be deeply involved in tumor progression, and we propose that segregation of transcripts into IMP3 RNPs may be a general mechanism that prevents miRNA-dependent mRNA decay during tumor growth.

EXPERIMENTAL PROCEDURES

Tumor Gene-Expression Profiles

Expression profiles of tumor samples were downloaded from the Gene Expression Omnibus (GEO) (http://www.ncbi.nlm.nih.gov/geo/) or generated from samples collected and processed at our own facility at Rigshospitalet. All tumors were analyzed on human U133 Plus 2.0 arrays (Affymetrix). Cell files were preprocessed using the robust multichip average (RMA) method (Bolstad et al., 2003) and evaluated for quality parameters using the Simpleaffy functionality of the *R/Bioconductor* packages. The data were visualized and analyzed using the Qlucore Omics Explorer software, and the probe sets employed in the two-way comparison and Pearson correlation coefficient were *IMP3* (203820_s_at) and *HMGA2* (208025_s_at).

Inhibition of *let-7* Family Members

A mixture of LNA antagomiRs was produced to specifically inhibit all members of the *let-7* family of miRNAs. The mixture consisted of five custom-designed LNA-containing oligonucleotides (*hsa-let-7a-d* CAACCTACTACCTC, *hsa-let-7e* ACAACCTCCTACCTC, *hsa-let-7f* ACAATCTACTACCTC, *hsa-let-7g-i* ACAAACTACTACCTCA, and *hsa-miR-98* CAACTTACTACCTCA). Upon transfection of the *let-7* family inhibitor mixture (50 nM) into TREX1080 3xFLAG-IMP3 cells, tetracycline was added to induce transcription of the 3xFLAG-IMP3 construct. As control, an LNA inhibitor against *miR-449b* was used (CCAGCTAACAATACACTGCCT). Transfections were performed with Turbofect (Fermentas). Cells were harvested 24 hr after transfection and subsequently lysed in TriZol (Invitrogen).

Isolation of 3xFLAG-IMP3 and Ago2 RNPs

Anti-Ago2 agarose beads were prepared with protein A/G and the 4F11 Ago2 antibody (Rüdel et al., 2008), and immunoprecipitation of 3xFLAG-IMP3 was performed as previously described using anti-FLAG agarose beads from Sigma-Aldrich (Jønson et al., 2011).

SHAPE Probing

For SHAPE probing, 10 nM of *HMGA2* 3′ UTR segment 1,088–1,306 was renatured in 20 mM Tris-HCl, pH 7.8, 140 mM KCl, 2 mM $MgCl_2$, and 0.1% Triton X-100 by heating at 90°C for 1 min and at 56°C for 10 min, followed by the addition of 0.4 U/μl RNasin and 2 mM dithiothreitol. Binding of 30 nM recombinant IMP3 to renatured RNA was carried out at 30°C for 20 min, and 30 nM *let-7*g miRNA was subsequently added for 10 min. The acylation reaction by 8 mM 1-methyl-7-nitroisatoic anhydride (1M7) proceeded for 70 s at room temperature, and the reaction was stopped by the addition of water. Analysis of acylation reactions and dideoxynucleoside sequencing tracks were obtained by reverse transcription initiated by a 5′ end-labeled primer complementary to *HMGA2* 3′ UTR positions 1,283–1,306 as described previously (Nielsen and Christiansen, 1992).

Whole-Mount RNA In Situ Hybridization

Whole-mount RNA in situ hybridization was performed as previously described (Hansen et al., 2004). In brief, embryos were fixed overnight in 4% paraformaldehyde at 4°C. After three washes in PBT (PBS plus 1% Tween 20), the embryos were rehydrated in a series of methanol-PBT, bleached in 6% hydrogen peroxide, and treated with proteinase K (Roche). The embryos were prehybridized in hybridization buffer containing yeast tRNA and hybridized at 65°C overnight in hybridization buffer containing 1 μg/ml of *Hmga2* or *Imp1* digoxigenin-labeled antisense riboprobe. After hybridization, the embryos were washed in RNaseA-containing wash buffer. The transcripts were detected by overnight incubation with digoxigenin antibody (Roche).

SUPPLEMENTAL INFORMATION

Supplemental Information includes Supplemental Experimental Procedures and six figures and can be found with this article online at http://dx.doi.org/10.1016/j.celrep.2014.03.015.

ACKNOWLEDGMENTS

We thank Lis Schutt Nielsen, Stine Østergaard, Susanne Smed, and Lena Bjørn Johansson for technical assistance and Dr. Jens Lykke-Andersen for supplying the DCP1a antibody. This study was supported by grants from the Danish Medical and Strategic Research Councils, the Svend Andersen Foundation, the Toyota Foundation, and the Lundbeck Foundation.

Received: July 1, 2013
Revised: January 28, 2014
Accepted: March 6, 2014
Published: April 3, 2014

REFERENCES

Beljan Perak, R., Durdov, M.G., Capkun, V., Ivcevic, V., Pavlovic, A., Soljic, V., and Peric, M. (2012). IMP3 can predict aggressive behaviour of lung adenocarcinoma. Diagn. Pathol. *7*, 165.

Bellezza, G., Cavaliere, A., and Sidoni, A. (2009). IMP3 expression in non-small cell lung cancer. Hum. Pathol. *40*, 1205–1206.

Bolstad, B.M., Irizarry, R.A., Astrand, M., and Speed, T.P. (2003). A comparison of normalization methods for high density oligonucleotide array data based on variance and bias. Bioinformatics *19*, 185–193.

Boyerinas, B., Park, S.M., Shomron, N., Hedegaard, M.M., Vinther, J., Andersen, J.S., Feig, C., Xu, J., Burge, C.B., and Peter, M.E. (2008). Identification of let-7-regulated oncofetal genes. Cancer Res. *68*, 2587–2591.

Brants, J.R., Ayoubi, T.A., Chada, K., Marchal, K., Van de Ven, W.J., and Petit, M.M. (2004). Differential regulation of the insulin-like growth factor II mRNA-binding protein genes by architectural transcription factor HMGA2. FEBS Lett. *569*, 277–283.

Chen, S.T., Jeng, Y.M., Chang, C.C., Chang, H.H., Huang, M.C., Juan, H.F., Hsu, C.H., Lee, H., Liao, Y.F., Lee, Y.L., et al. (2011). Insulin-like growth factor II mRNA-binding protein 3 expression predicts unfavorable prognosis in patients with neuroblastoma. Cancer Sci. *102*, 2191–2198.

Chen, Y.L., Jeng, Y.M., Hsu, H.C., Lai, H.S., Lee, P.H., Lai, P.L., and Yuan, R.H. (2013). Expression of insulin-like growth factor II mRNA-binding protein 3 predicts early recurrence and poor prognosis in intrahepatic cholangiocarcinoma. Int. J. Surg. *11*, 85–91.

Chiappetta, G., Avantaggiato, V., Visconti, R., Fedele, M., Battista, S., Trapasso, F., Merciai, B.M., Fidanza, V., Giancotti, V., Santoro, M., et al. (1996). High level expression of the HMGI (Y) gene during embryonic development. Oncogene *13*, 2439–2446.

Christiansen, J., Kolte, A.M., Hansen, Tv., and Nielsen, F.C. (2009). IGF2 mRNA-binding protein 2: biological function and putative role in type 2 diabetes. J. Mol. Endocrinol. *43*, 187–195.

Cleynen, I., and Van de Ven, W.J. (2008). The HMGA proteins: a myriad of functions (Review). Int. J. Oncol. *32*, 289–305.

Dogar, A.M., Semplicio, G., Guennewig, B., and Hall, J. (2014). Multiple microRNAs derived from chemically synthesized precursors regulate thrombospondin 1 expression. Nucleic Acid Ther., Published online January 20, 2014. 10.1089.

Elcheva, I., Goswami, S., Noubissi, F.K., and Spiegelman, V.S. (2009). CRD-BP protects the coding region of betaTrCP1 mRNA from miR-183-mediated degradation. Mol. Cell *35*, 240–246.

Findeis-Hosey, J.J., Yang, Q., Spaulding, B.O., Wang, H.L., and Xu, H. (2010). IMP3 expression is correlated with histologic grade of lung adenocarcinoma. Hum. Pathol. *41*, 477–484.

Fusco, A., and Fedele, M. (2007). Roles of HMGA proteins in cancer. Nat. Rev. Cancer *7*, 899–910.

Gallagher, I.J., Scheele, C., Keller, P., Nielsen, A.R., Remenyi, J., Fischer, C.P., Roder, K., Babraj, J., Wahlestedt, C., Hutvagner, G., et al. (2010). Integration of microRNA changes in vivo identifies novel molecular features of muscle insulin resistance in type 2 diabetes. Genome Med. *2*, 9.

Han, T.W., Kato, M., Xie, S., Wu, L.C., Mirzaei, H., Pei, J., Chen, M., Xie, Y., Allen, J., Xiao, G., and McKnight, S.L. (2012). Cell-free formation of RNA granules: bound RNAs identify features and components of cellular assemblies. Cell *149*, 768–779.

Hansen, T.V., Hammer, N.A., Nielsen, J., Madsen, M., Dalbaeck, C., Wewer, U.M., Christiansen, J., and Nielsen, F.C. (2004). Dwarfism and impaired gut development in insulin-like growth factor II mRNA-binding protein 1-deficient mice. Mol. Cell. Biol. *24*, 4448–4464.

Hartmann, E.M., Beà, S., Navarro, A., Trapp, V., Campo, E., Ott, G., and Rosenwald, A. (2012). Increased tumor cell proliferation in mantle cell lymphoma is associated with elevated insulin-like growth factor 2 mRNA-binding protein 3 expression. Mod. Pathol. *25*, 1227–1235.

Heo, I., Joo, C., Cho, J., Ha, M., Han, J., and Kim, V.N. (2008). Lin28 mediates the terminal uridylation of let-7 precursor MicroRNA. Mol. Cell *32*, 276–284.

Hoffmann, N.E., Sheinin, Y., Lohse, C.M., Parker, A.S., Leibovich, B.C., Jiang, Z., and Kwon, E.D. (2008). External validation of IMP3 expression as an independent prognostic marker for metastatic progression and death for patients with clear cell renal cell carcinoma. Cancer *112*, 1471–1479.

Hu, X., Guo, J., Zheng, L., Li, C., Zheng, T.M., Tanyi, J.L., Liang, S., Benedetto, C., Mitidieri, M., Katsaros, D., et al. (2013). The heterochronic microRNA let-7 inhibits cell motility by regulating the genes in the actin cytoskeleton pathway in breast cancer. Mol. Cancer Res. *11*, 240–250.

Jeng, Y.M., Chang, C.C., Hu, F.C., Chou, H.Y., Kao, H.L., Wang, T.H., and Hsu, H.C. (2008). RNA-binding protein insulin-like growth factor II mRNA-binding protein 3 expression promotes tumor invasion and predicts early recurrence and poor prognosis in hepatocellular carcinoma. Hepatology *48*, 1118–1127.

Jiang, Z., Chu, P.G., Woda, B.A., Liu, Q., Balaji, K.C., Rock, K.L., and Wu, C.L. (2008a). Combination of quantitative IMP3 and tumor stage: a new system to predict metastasis for patients with localized renal cell carcinomas. Clin. Cancer Res. *14*, 5579–5584.

Jiang, Z., Lohse, C.M., Chu, P.G., Wu, C.L., Woda, B.A., Rock, K.L., and Kwon, E.D. (2008b). Oncofetal protein IMP3: a novel molecular marker that predicts metastasis of papillary and chromophobe renal cell carcinomas. Cancer *112*, 2676–2682.

Jønson, L., Vikesaa, J., Krogh, A., Nielsen, L.K., Hansen, Tv., Borup, R., Johnsen, A.H., Christiansen, J., and Nielsen, F.C. (2007). Molecular composition of IMP1 ribonucleoprotein granules. Mol. Cell. Proteomics *6*, 798–811.

Jønson, L., Nielsen, F.C., and Christiansen, J. (2011). Isolation of RNP granules. Methods Mol. Biol. *703*, 265–273.

Kapoor, S. (2008). IMP3: a new and important biomarker of systemic malignancies. Clin. Cancer Res. *14*, 5640, author reply 5640–5641.

Kato, M., Han, T.W., Xie, S., Shi, K., Du, X., Wu, L.C., Mirzaei, H., Goldsmith, E.J., Longgood, J., Pei, J., et al. (2012). Cell-free formation of RNA granules: low complexity sequence domains form dynamic fibers within hydrogels. Cell *149*, 753–767.

Kim, K.Y., and Cha, I.H. (2011). A novel algorithm for lymph node status prediction of oral cancer before surgery. Oral Oncol. *47*, 1069–1073.

Kim, K.Y., Li, S., Cha, J.D., Zhang, X., and Cha, I.H. (2012). Significance of molecular markers in survival prediction of oral squamous cell carcinoma. Head Neck *34*, 929–936.

Köbel, M., Xu, H., Bourne, P.A., Spaulding, B.O., Shih, IeM., Mao, T.L., Soslow, R.A., Ewanowich, C.A., Kalloger, S.E., Mehl, E., et al. (2009). IGF2BP3 (IMP3) expression is a marker of unfavorable prognosis in ovarian carcinoma of clear cell subtype. Mod. Pathol. *22*, 469–475.

Lee, Y.S., and Dutta, A. (2007). The tumor suppressor microRNA let-7 represses the HMGA2 oncogene. Genes Dev. *21*, 1025–1030.

Li, S., Cha, J., Kim, J., Kim, K.Y., Kim, H.J., Nam, W., and Cha, I.H. (2011). Insulin-like growth factor II mRNA-binding protein 3: a novel prognostic biomarker for oral squamous cell carcinoma. Head Neck *33*, 368–374.

Li, Z., Gilbert, J.A., Zhang, Y., Zhang, M., Qiu, Q., Ramanujan, K., Shavlakadze, T., Eash, J.K., Scaramozza, A., Goddeeris, M.M., et al. (2012). An HMGA2-IGF2BP2 axis regulates myoblast proliferation and myogenesis. Dev. Cell *23*, 1176–1188.

Lochhead, P., Imamura, Y., Morikawa, T., Kuchiba, A., Yamauchi, M., Liao, X., Qian, Z.R., Nishihara, R., Wu, K., Meyerhardt, J.A., et al. (2012). Insulin-like growth factor 2 messenger RNA binding protein 3 (IGF2BP3) is a marker of unfavourable prognosis in colorectal cancer. Eur. J. Cancer *48*, 3405–3413.

Lu, D., Yang, X., Jiang, N.Y., Woda, B.A., Liu, Q., Dresser, K., Mercurio, A.M., Rock, K.L., and Jiang, Z. (2011). IMP3, a new biomarker to predict progression of cervical intraepithelial neoplasia into invasive cancer. Am. J. Surg. Pathol. *35*, 1638–1645.

Mayr, C., Hemann, M.T., and Bartel, D.P. (2007). Disrupting the pairing between let-7 and Hmga2 enhances oncogenic transformation. Science *315*, 1576–1579.

McGinnis, J.L., Dunkle, J.A., Cate, J.H., and Weeks, K.M. (2012). The mechanisms of RNA SHAPE chemistry. J. Am. Chem. Soc. *134*, 6617–6624.

Mentrikoski, M.J., Ma, L., Pryor, J.G., McMahon, L.A., Yang, Q., Spaulding, B.O., Scott, G.A., Wang, H.L., and Xu, H. (2009). Diagnostic utility of IMP3 in segregating metastatic melanoma from benign nevi in lymph nodes. Mod. Pathol. *22*, 1582–1587.

Mhawech-Fauceglia, P., Herrmann, F.R., Rai, H., Tchabo, N., Lele, S., Izevbaye, I., Odunsi, K., and Cheney, R.T. (2010). IMP3 distinguishes uterine serous carcinoma from endometrial endometrioid adenocarcinoma. Am. J. Clin. Pathol. *133*, 899–908.

Molenaar, J.J., Domingo-Fernández, R., Ebus, M.E., Lindner, S., Koster, J., Drabek, K., Mestdagh, P., van Sluis, P., Valentijn, L.J., van Nes, J., et al. (2012). LIN28B induces neuroblastoma and enhances MYCN levels via let-7 suppression. Nat. Genet. *44*, 1199–1206.

Nielsen, F.C., and Christiansen, J. (1992). Endonucleolysis in the turnover of insulin-like growth factor II mRNA. J. Biol. Chem. *267*, 19404–19411.

Nielsen, J., Christiansen, J., Lykke-Andersen, J., Johnsen, A.H., Wewer, U.M., and Nielsen, F.C. (1999). A family of insulin-like growth factor II mRNA-binding proteins represses translation in late development. Mol. Cell. Biol. *19*, 1262–1270.

Nielsen, F.C., Nielsen, J., and Christiansen, J. (2001). A family of IGF-II mRNA binding proteins (IMP) involved in RNA trafficking. Scand. J. Clin. Lab. Invest. Suppl. *234*, 93–99.

Nielsen, F.C., Nielsen, J., Kristensen, M.A., Koch, G., and Christiansen, J. (2002). Cytoplasmic trafficking of IGF-II mRNA-binding protein by conserved KH domains. J. Cell Sci. *115*, 2087–2097.

Nielsen, J., Kristensen, M.A., Willemoës, M., Nielsen, F.C., and Christiansen, J. (2004). Sequential dimerization of human zipcode-binding protein IMP1 on RNA: a cooperative mechanism providing RNP stability. Nucleic Acids Res. *32*, 4368–4376.

Park, S.M., Shell, S., Radjabi, A.R., Schickel, R., Feig, C., Boyerinas, B., Dinulescu, D.M., Lengyel, E., and Peter, M.E. (2007). Let-7 prevents early cancer progression by suppressing expression of the embryonic gene HMGA2. Cell Cycle *6*, 2585–2590.

Rüdel, S., Flatley, A., Weinmann, L., Kremmer, E., and Meister, G. (2008). A multifunctional human Argonaute2-specific monoclonal antibody. RNA *14*, 1244–1253.

Runge, S., Nielsen, F.C., Nielsen, J., Lykke-Andersen, J., Wewer, U.M., and Christiansen, J. (2000). H19 RNA binds four molecules of insulin-like growth factor II mRNA-binding protein. J. Biol. Chem. *275*, 29562–29569.

Schaeffer, D.F., Owen, D.R., Lim, H.J., Buczkowski, A.K., Chung, S.W., Scudamore, C.H., Huntsman, D.G., Ng, S.S., and Owen, D.A. (2010). Insulin-like growth factor 2 mRNA binding protein 3 (IGF2BP3) overexpression in

pancreatic ductal adenocarcinoma correlates with poor survival. BMC Cancer *10*, 59.

Schmitter, D., Filkowski, J., Sewer, A., Pillai, R.S., Oakeley, E.J., Zavolan, M., Svoboda, P., and Filipowicz, W. (2006). Effects of Dicer and Argonaute down-regulation on mRNA levels in human HEK293 cells. Nucleic Acids Res. *34*, 4801–4815.

Shinoda, G., Shyh-Chang, N., de Soysa, T.Y., Zhu, H., Seligson, M.T., Shah, S.P., Abo-Sido, N., Yabuuchi, A., Hagan, J.P., Gregory, R.I., et al. (2013). Fetal deficiency of Lin28 programs life-long aberrations in growth and glucose metabolism. Stem Cells *31*, 1563–1573.

Sitnikova, L., Mendese, G., Liu, Q., Woda, B.A., Lu, D., Dresser, K., Mohanty, S., Rock, K.L., and Jiang, Z. (2008). IMP3 predicts aggressive superficial urothelial carcinoma of the bladder. Clin. Cancer Res. *14*, 1701–1706.

Speese, S.D., Ashley, J., Jokhi, V., Nunnari, J., Barria, R., Li, Y., Ataman, B., Koon, A., Chang, Y.T., Li, Q., et al. (2012). Nuclear envelope budding enables large ribonucleoprotein particle export during synaptic Wnt signaling. Cell *149*, 832–846.

Szarvas, T., vom Dorp, F., Niedworok, C., Melchior-Becker, A., Fischer, J.W., Singer, B.B., Reis, H., Bánkfalvi, A., Schmid, K.W., Romics, I., et al. (2012). High insulin-like growth factor mRNA-binding protein 3 (IMP3) protein expression is associated with poor survival in muscle-invasive bladder cancer. BJU Int. *110* (6 Pt B), E308–E317.

Tessier, C.R., Doyle, G.A., Clark, B.A., Pitot, H.C., and Ross, J. (2004). Mammary tumor induction in transgenic mice expressing an RNA-binding protein. Cancer Res. *64*, 209–214.

Thornton, J.E., and Gregory, R.I. (2012). How does Lin28 let-7 control development and disease? Trends Cell Biol. *22*, 474–482.

van Kouwenhove, M., Kedde, M., and Agami, R. (2011). MicroRNA regulation by RNA-binding proteins and its implications for cancer. Nat. Rev. Cancer *11*, 644–656.

Viswanathan, S.R., Daley, G.Q., and Gregory, R.I. (2008). Selective blockade of microRNA processing by Lin28. Science *320*, 97–100.

Viswanathan, S.R., Powers, J.T., Einhorn, W., Hoshida, Y., Ng, T.L., Toffanin, S., O'Sullivan, M., Lu, J., Phillips, L.A., Lockhart, V.L., et al. (2009). Lin28 promotes transformation and is associated with advanced human malignancies. Nat. Genet. *41*, 843–848.

Wagner, M., Kunsch, S., Duerschmied, D., Beil, M., Adler, G., Mueller, F., and Gress, T.M. (2003). Transgenic overexpression of the oncofetal RNA binding protein KOC leads to remodeling of the exocrine pancreas. Gastroenterology *124*, 1901–1914.

Walter, O., Prasad, M., Lu, S., Quinlan, R.M., Edmiston, K.L., and Khan, A. (2009). IMP3 is a novel biomarker for triple negative invasive mammary carcinoma associated with a more aggressive phenotype. Hum. Pathol. *40*, 1528–1533.

Weber, S.C., and Brangwynne, C.P. (2012). Getting RNA and protein in phase. Cell *149*, 1188–1191.

Yang, D.H., and Moss, E.G. (2003). Temporally regulated expression of Lin-28 in diverse tissues of the developing mouse. Gene Expr. Patterns *3*, 719–726.

Yantiss, R.K., Cosar, E., and Fischer, A.H. (2008). Use of IMP3 in identification of carcinoma in fine needle aspiration biopsies of pancreas. Acta Cytol. *52*, 133–138.

Yuan, R.H., Wang, C.C., Chou, C.C., Chang, K.J., Lee, P.H., and Jeng, Y.M. (2009). Diffuse expression of RNA-binding protein IMP3 predicts high-stage lymph node metastasis and poor prognosis in colorectal adenocarcinoma. Ann. Surg. Oncol. *16*, 1711–1719.

Yun, J., Frankenberger, C.A., Kuo, W.L., Boelens, M.C., Eves, E.M., Cheng, N., Liang, H., Li, W.H., Ishwaran, H., Minn, A.J., and Rosner, M.R. (2011). Signalling pathway for RKIP and Let-7 regulates and predicts metastatic breast cancer. EMBO J. *30*, 4500–4514.

Zhou, X., Benson, K.F., Ashar, H.R., and Chada, K. (1995). Mutation responsible for the mouse pygmy phenotype in the developmentally regulated factor HMGI-C. Nature *376*, 771–774.

Zhu, H., Shyh-Chang, N., Segrè, A.V., Shinoda, G., Shah, S.P., Einhorn, W.S., Takeuchi, A., Engreitz, J.M., Hagan, J.P., Kharas, M.G., et al.; DIAGRAM Consortium; MAGIC Investigators. (2011). The Lin28/let-7 axis regulates glucose metabolism. Cell *147*, 81–94.